IEEE Access
Multidisciplinary | Rapid Review | Open Access Journal

Received December 25, 2021, accepted January 10, 2022, date of publication January 14, 2022, date of current version January 21, 2022.

Digital Object Identifier 10.1109/ACCESS.2022.3143794

Analysis of a Discrete Stator Hybrid Excited Flux Switching Linear Machine

BASHARAT ULLAH[1], (Graduate Student Member, IEEE), FAISAL KHAN[1], (Member, IEEE), AND AHMAD H. MILYANI[2]

[1]Department of Electrical and Computer Engineering, COMSATS University Islamabad, Abbottabad 22060, Pakistan
[2]Department of Electrical and Computer Engineering, King Abdulaziz University, Jeddah 21589, Saudi Arabia

Corresponding author: Basharat Ullah (basharat.bigb@gmail.com)

This work was supported in part by COMSATS University Islamabad, Abbottabad Campus; and in part by the Higher Education Commission of Pakistan under Grant TDF-03-067/R&D/HEC/2019.

ABSTRACT A discrete stator hybrid excited flux switching linear machine (DSHEFSLM) is proposed in this paper. The proposed DSHEFSLM uses a discrete stator to reduce the iron loss and overall cost of the machine. Assistant teeth are used at both ends of the mover to overcome the unbalance in the three phases, which is a global issue in linear machines. Field excitation (FE) is used, which adds field regulation capability to the proposed machine and makes it suitable for a wide speed operation range. A magnetic equivalent circuit model is used to find the suitable coil combination and no-load flux linkage. The multiobjective genetic global optimization is used to optimize the design parameters of the whole machine while keeping the slot area, electric and magnetic loadings constant. A correlation table is drawn to show the impact of different design parameters on average thrust force. The optimization has increased the peak-to-peak flux linkage by 11%, average thrust force by 34.60%, thrust force density by 34.60%, decreased thrust force ripples, and detent force by 21.05% and 8.58% respectively. The proposed machine has reduced the volume of the permanent magnet by 39.18% and offers 28.09% higher average thrust force and thrust force density compared to the flux switching permanent magnet machine proposed in the literature.

INDEX TERMS Discrete stator, finite element analysis, flux switching machine, series hybridization, linear machines, variable flux machine.

NOMENCLATURE

β	materials constant.
μ_r	relative permeability.
ϕ_s	flux source.
B_i	magnetic flux density.
B_r	PM remanence.
F	magneto motive force (mmf).
F_i	magnetic potential drop.
F_{FE}	FEC mmf.
F_{pm}	PM mmf.
H_i	magnetic field intensity.
l_i	length of iron part.
l_{pm}	length of PM.
M_s	magnetization saturation.
P	permeance.
P_a	air gap permeance.
P_m	mover core permeance.
P_{pm}	PM permeance.
P_s	stator core permeance.

The associate editor coordinating the review of this manuscript and approving it for publication was Wei Xu.

I. INTRODUCTION

Linear machines are in high demand in various applications, ranging from domestic applications to industrialization. Linear machines are preferred over rotary machines because they produce force directly along the x-axis with higher efficiency, reliability, and less energy loss.

Machines with permanent magnet (PM) on a short mover are gaining popularity due to their advantages of high power density and efficiency [1]. PM flux switching linear (PMFSL), PM doubly salient linear (PMDSL), and PM flux reversal linear (PMFRL) machines are examples of mover-mounted PM machines. PMFSL machine combines the characteristics of PM synchronous linear machines (PMSLM) and switched reluctance linear machines (SRLM). PMFSL machine has high power density [2],

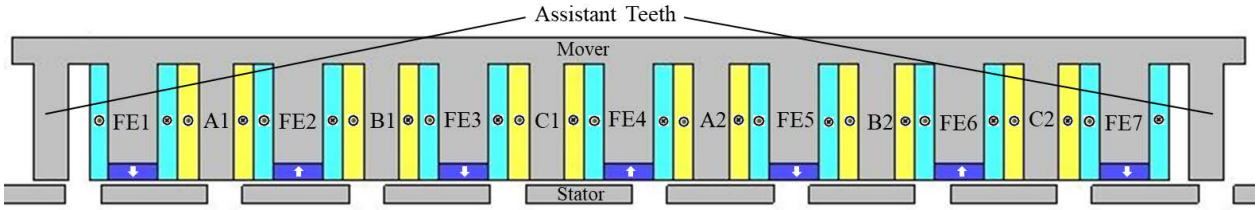

FIGURE 1. Design of proposed DSHEFSLM.

bipolar flux linkage, and a rugged stator, making it suitable for high-speed long stroke applications [3]. Additionally, improved temperature control has reduced manufacturing costs [4] and is compatible with extreme environmental conditions [5].

However, the unregulated PM flux of the PMFSL machine limits its speed range. The alternate choice is the field excited flux switching linear (FEFSL) machine, which offers a wide speed range based on variation in field current. But the FEFSL machine suffers from low flux linkage and has lower thrust force density than PMFSL machines. To overcome the disadvantages of PMFSL and FEFSL machines, hybrid excited flux switching linear (HEFSL) machines are proposed, which possess better flux linkage, high thrust force density, and better flux controlling ability [4]. The authors in [1], [4], [6]–[22] proposed and investigated numerous hybrid excited rotary and linear topologies. Based on the rotating hybrid excited flux switching machine suggested in [4], [6] proposed and investigated a new type of HEFSL machine which replace the rare earth PMs with ferrite magnets and to improve flux modulation, additional field excitation (FE) windings are used. After that, the proposed HEFSL is transformed into a double-sided HEFSL machine [9]. Three possible types of hybrid excited flux switching (HEFS) rotary topologies with FE coils situated in stator slots are proposed and researched in [7]. Three FSHE machines based on the positioning of PMs at the bottom, middle and top are proposed in [11]. The investigation showed that the bottom PM has the best use of the PM and flux regulating ability.

A new partitioned primary, segmented stator HEFSL machine is proposed in [23], [24] having separate field and armature windings, which help in good temperature distribution. However, they have poor flux linkage due to large flux linking paths and have a flux circulation problem. In [25], a slot PM machine is proposed with concentrated field and armature winding hence low copper losses and good efficiency, but it has problems of magnetic saturation, flux leakage, and rare earth magnets are used in substantial volume. Another HEFSL machine is proposed in [17] in which the PM is sandwiched between two DC excitation sources and is converted into dual mover topology in [19].

This paper proposes a series hybridized discrete stator hybrid excited flux switching linear machine (DSHEFSLM), which is based on the PMFSL machine proposed in [26]. The proposed machine has reduced the volume of PM by 39.18% and offers a 28.09% higher average thrust force and thrust force density. Furthermore, the proposed design uses FE windings which adds flux regulation capability and make it suitable for wide-speed applications like electric power train. In the rest of the paper, section II introduces the machine topology and its working principle; the magnetic equivalent model is employed in section III to find suitable coil combinations and find the machine's initial performance. Genetic optimization is done in section IV, while simulation results obtained by finite element analysis (FEA) are discussed in section V. Finally, section VI concludes the paper.

II. MACHINE TOPOLOGY AND WORKING PRINCIPLE

The proposed DSHEFSLM is shown in Fig. 1. The proposed design has a discrete stator that reduces iron consumption and iron losses in the stator. Mover contains all the excitation sources. PMs are placed at the alternate pole tip of the mover. Three-phase concentrated armature windings are used and are wound on the iron teeth. Each phase is composed of two sets of armature coils. Field excitation windings are used and wound on the mover teeth containing PMs, which provides series hybridization. The leading design parameters are given in Table 1 and denoted in Fig. 2.

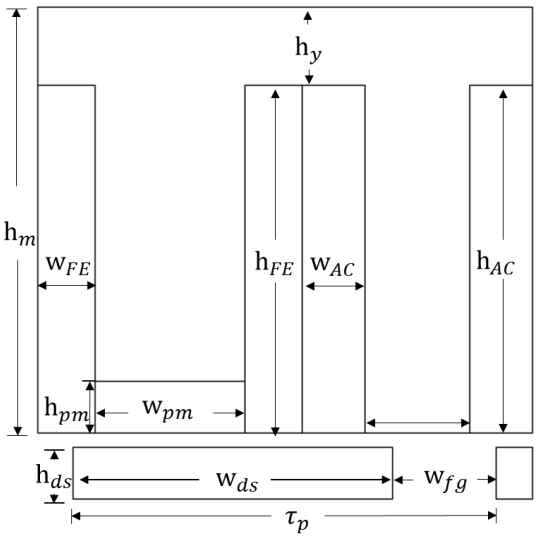

FIGURE 2. Geometry parameters representation.

The working principle of the proposed design is based on a no-load flux linkage obtained by a magnetic equivalent model (MEM) and verified by 2D FEA. The flux produced

TABLE 1. Geometry parameters of DSHEFSLM.

Parameter	Symbol	VAlue
mover height	h_m	24.5 mm
iron tooth width	w_{it}	6.01 mm
AC slot height	h_{AE}	20 mm
PM height	h_{PM}	3 mm
Rated velocity	ν	2 m/sec
air gap	A_g	0.8 mm
stack length	L	160 mm
stator pole pitch	τ_p	24.36 mm
mover pole pitch	τ_s	14.21 mm
stator piece width	w_ds	18 mm
winding filling factor	α	0.5
armature turns	N_A	38
rated current	I_A	15 A
FE current	I_{FE}	6 A

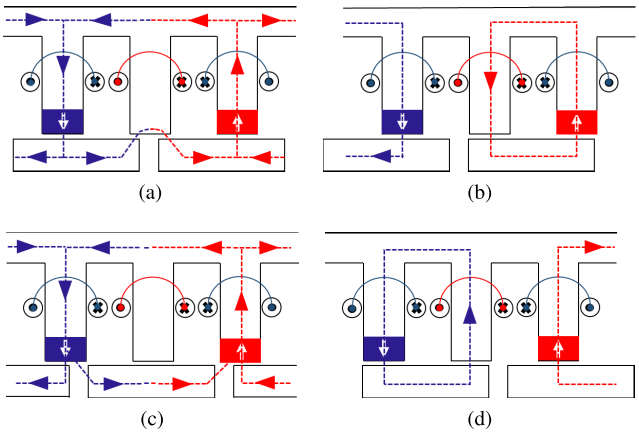

FIGURE 3. (a) Mover at position *a* (b) Mover at position *b* (c) Mover at position *c* (d) Mover at position *d*.

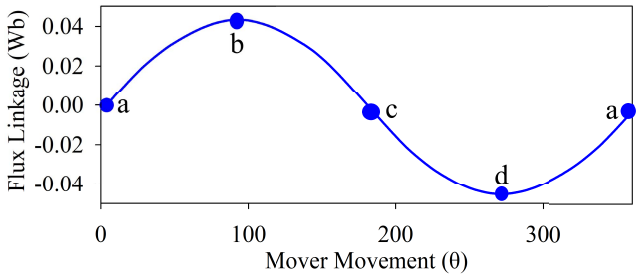

FIGURE 4. No-load flux linkage of single phase.

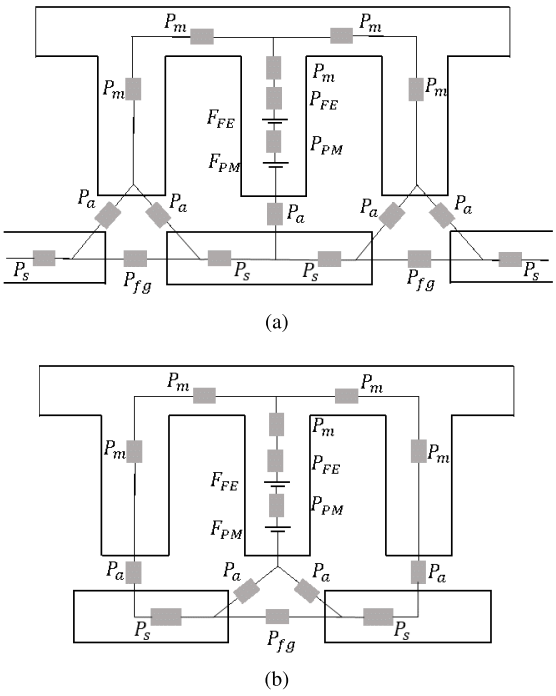

FIGURE 5. MEM of the proposed model with (a) mover at position *a* (b) mover at position *b*.

by FE and PM goes pass through the mover tooth containing PM crosses air gap enters stator body and leaves immediately, passes again across the air gap and enters the subsequent mover tooth i.e. the iron tooth, passes through mover's yoke and complete its circuit. This all can be evident from Fig. 3. If the flux and armature coil are in the same direction (Fig. 3b) then the flux attains maximum positive value shown by point *b* in Fig. 4, and negative maximum if both are in opposite direction (Fig. 3d) shown by point *d* in Fig. 4. When the mover is at positions *a* (Fig. 3a) and *c* (Fig. 3c), the flux does not pass through the iron tooth having armature winding, so the net flux linkage in the coil becomes zero shown by point *a* and *c* in the Fig. 4. Due to symmetry, the cycle repeats itself.

III. MAGNETIC EQUIVALENT MODEL

To reduce the computational complexity and drive storage, MEM is used to find initial performance and suitable coil combinations for the proposed design. As MEM models all parts of the machine like stator, air gap, and mover, it gives better results in terms of accuracy. In the case of the proposed machine, two magnetic equivalent models are developed based on the position of mover shown in Fig. 5. The models are developed considering one magnet magnetized and extended to the whole machine to reduce the computational time and drive storage. The model formulations are based on the following equations [21]:

$$\phi_s = PF \tag{1}$$

$$F_{PM} = \frac{B_r l_{pm}}{\mu_o \mu_r} \tag{2}$$

$$F_{FE} = N_{FE} I_{FE} \tag{3}$$

$$P_{PM} = \frac{\mu_o \mu_r l_{stk} w_{pm}}{l_{pm}} \tag{4}$$

The permeance of iron parts can be calculated as:

$$P_{m/s} = \int \frac{\mu_o \mu_r}{l_i} dA_i \tag{5}$$

TABLE 2. Computational time and drive storage comparison.

Method Used	Time	Drive Storage
MEM	6.22 s	189 KBs
2D FEA	6 min and 51 s	205 MBs

After calculating the permeance of all parts, and sources at nodes, nodal analysis is employed to calculate flux flowing out and flowing in to the corresponding nodes as:

$$\begin{bmatrix} \phi_s(1) \\ \vdots \\ \phi_s(N) \end{bmatrix} = \begin{bmatrix} P(1,1) & \cdots & P(1,N) \\ \vdots & \ddots & \vdots \\ P(M,1) & \cdots & P(M,N) \end{bmatrix} \begin{bmatrix} F(1) \\ \vdots \\ F(N) \end{bmatrix} \quad (6)$$

$P(M, N)$, the permeance matrix can be written as follows:

$$P(M,N) = \begin{cases} 1 & branch\ N\ begins\ from\ node\ M \\ 0 & no\ connection\ between\ branch\ N \\ & \quad and\ node\ M \\ -1 & branch\ N\ ends\ at\ \ node\ M \end{cases} \quad (7)$$

Eq. (6) is solved in three steps [27], through iterative process to calculate the no-load flux linkage with considering the initial relative permeability of 4000. Firstly, H_i in the mover and stator part is calculated using Eq. (8). Once H_i is calculated, relative permeability is updated using Eq. (9). Finally, magnetic flux density (Eq. (10)) is calculated using the same iterative process. Fig. 6 shows the no-load flux linkage obtained by FEA analysis and calculated through MEM. There is a small error between the two but considering computational time, drive storage it is not that significant.

$$H_i^{k-1} = \frac{\Delta F_i^{k-1}}{l_i} \quad (8)$$

$$\mu_r^k = \frac{\left[H_i^{k-1} + M_s\left(coth\left(\frac{H_i^{k-1}}{\beta}\right) - \frac{\beta}{H_i^{k-1}}\right)\right]}{H_i^{k-1}} \quad (9)$$

$$B_i^k = \frac{\Delta F_i^k P}{A_i} \quad (10)$$

The MEM is validated by JMAG v20.1 and detailed comparison based on computation time and drive storage is given in Table 2. The MEM greatly reduces the drive storage and computational time as compared to FEA. It is to mention that both MEM and FEA are done using 64 bit operating Lenovo system with 8 GB RAM, Intel(R), Core(TM) i5-8500 CPU 3.00GHz, 3000Mhz.

IV. GENETIC OPTIMIZATION

Genetic optimization (GO) is a heuristic search method that mimics the natural evolutionary process. This method is often used to generate useful solutions for optimization and search problems. GO does not rely on the initial (starting) point of the search, does not require any derivative information of the objective function or the constraint function, and is least likely to fall into a local minimum. The flowchart of GO

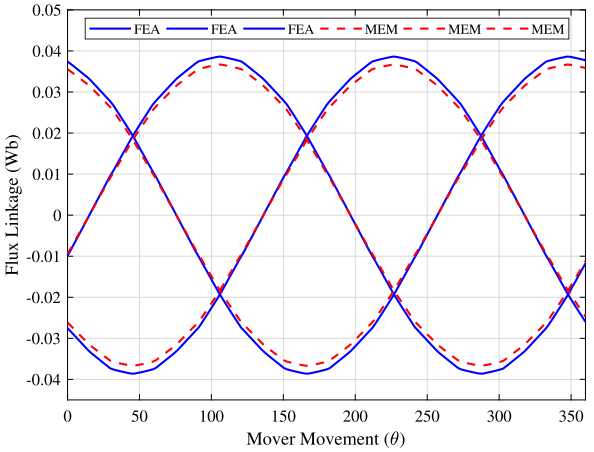

FIGURE 6. No-load flux linkages MEM vs FEA.

TABLE 3. Ranges of varying CAD parameters.

Variable	Initial Value	Constraint
w_{ds}	19.3 mm	[14-22]
h_{ds}	6 mm	[5-8.6]
A_{FE}	58.32 mm^2	[48-90]
A_{AC}	66 mm^2	[48-95]
A_{PM}	25 mm^2	[15-43]
h_y	4 mm	[2.5-8]

TABLE 4. Correlation of average thrust force with design variables.

Parameter	h_y	A_{pm}	A_{AC}	A_{FE}	h_{ds}	w_{ds}
TF_{avg}	-0.10	-0.05	-0.47	-0.43	0.23	0.18
TF_{rip}	0.12	0.17	0.39	0.28	-0.17	-0.26
F_d	0.12	0.23	0.29	0.35	-0.14	-0.29

used is shown in Fig. 7. Firstly, the initial design is made in geometry editor, and then the CAD parameters are imported to the designer. An objective function is defined in Eq. 11 comprises three sub objective functions, and the weighting factor is being specified based on the requirement. Ranges of varying CAD parameters and constraints are defined given in Table 3, to ensure constant electric and magnetic loadings. Number of generations and population size is initialized to achieve a global value of the objective function.

$$J_* = \lambda_1 \max(TF_{avg}) + \lambda_2 \min(TF_{rip}) + \lambda_3 \min(F_d) \quad (11)$$

TF_{avg} is the average thrust force, TF_{rip} are thrust force ripples, F_d is detent force and λ_1, λ_2, λ_3 are the weighting factors. The optimization problem of the proposed machine is the optimal solution of objective function based on the geometry design variables like split ratio ($S.R.$), yoke height (h_y), area of PM (A_{pm}), area of AC slot (A_{AC}), area of FE slot (A_{FE}), length of stator piece (w_{ds}), width of stator piece (h_{ds}) and width of the flux gap (w_{fg}). The main dimensions like mover height, mover pole pitch, air gap, stator pole pitch,

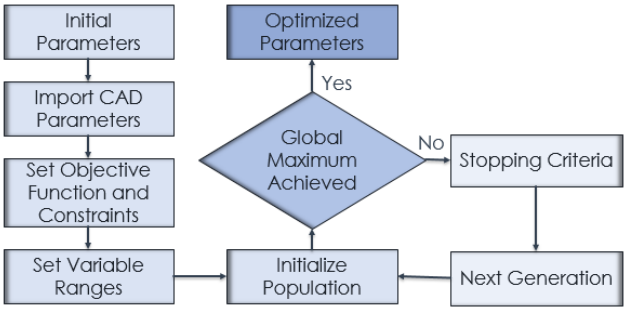

FIGURE 7. Flowchart.

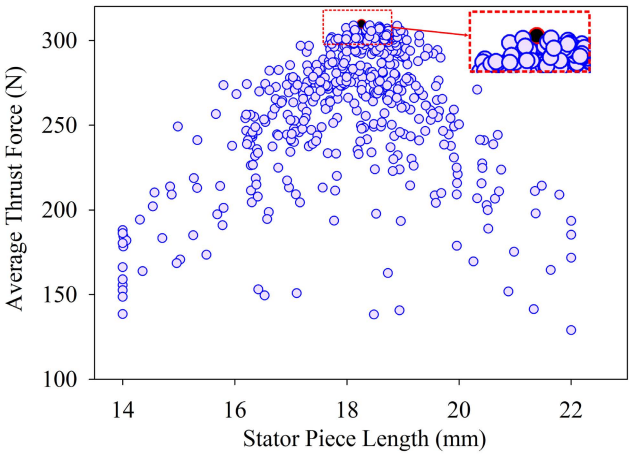

FIGURE 8. Stator piece length optimization.

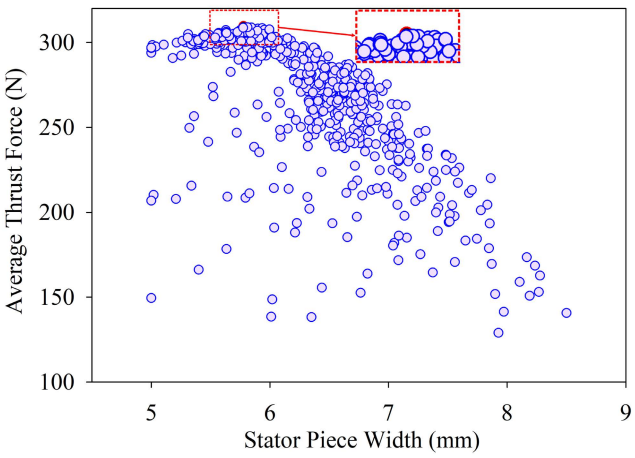

FIGURE 9. Stator piece width optimization.

stack length, rated current, and armature turns are kept constant during optimization. The correlation of average thrust force with different design variables is shown in Table 4.

Fig. 8 to Fig. 12 presents the TF_{avg} versus different geometry variables defined. From the figures, it can be seen that the TF_{avg} has achieved a global value of 313.5708N after the optimization, which is colored black and encircled red in all the figures. A detailed quantitative comparison Table 5 is drawn, which compares the initial and optimized design performances.

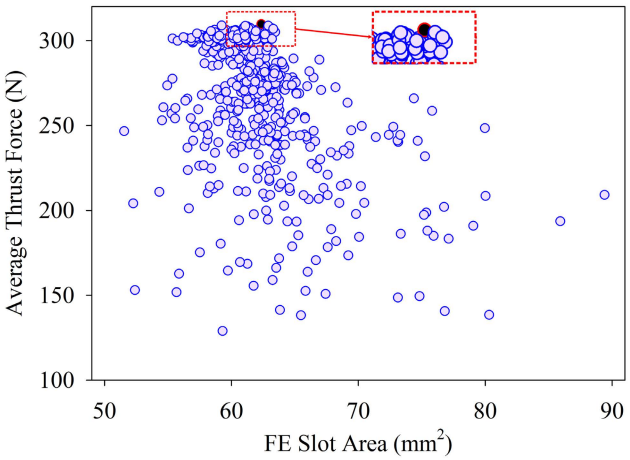

FIGURE 10. FE slot area optimization.

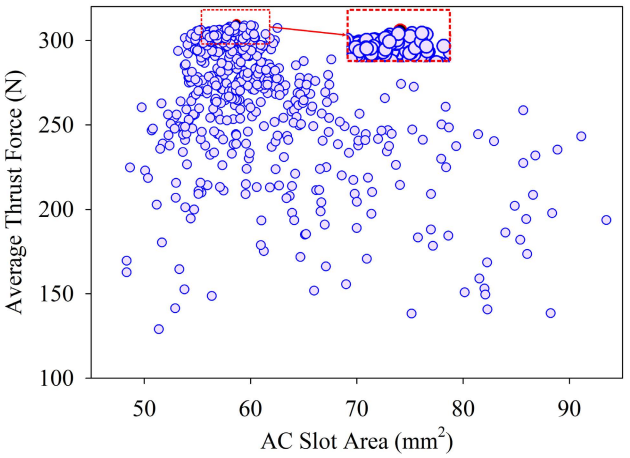

FIGURE 11. AC slot area optimization.

V. ELECTROMAGNETIC PERFORMANCE ANALYSIS

A. NO-LOAD ANALYSIS

The no-load flux linkage of the proposed DSHEFSLM design is shown in Fig. 13a, whereas Fig. 13b shows the harmonics. The flux linkage of all three phases is bipolar and sinusoidal. The impact of FE on the no-load flux linkage is shown in Fig. 14. Fig. 15 depicts the proposed machine's flux weakening and boosting capabilities at various FE current densities $J_e = 0, \pm 4, \pm 8, \pm 12$ (A/mm^2). The flux density in the air gap increases when the field current is positive, resulting in a stronger flux linkage; when the field current is negative, the flux density in the air gap decreases, resulting in a weaker flux linkage. The induced EMF can be calculated using Eq. 12 in which Φ represents the no-load flux linkage. Fig. 16a illustrates the back-EMF of the proposed DSHEFSLM at the velocity of $2m/s$. The harmonics of the back-EMF are given in Fig. 16b. The fundamental harmonic is important for

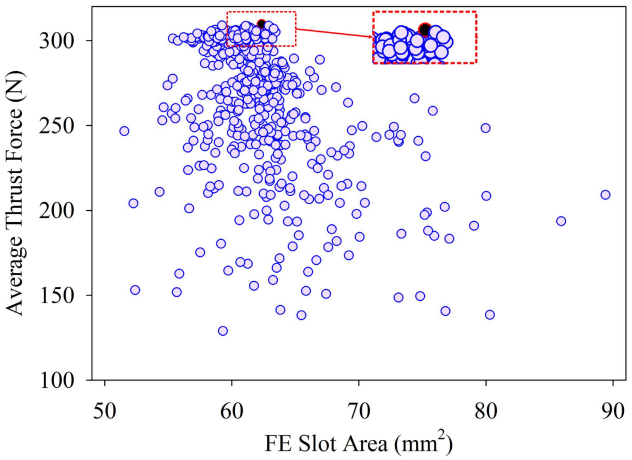

FIGURE 12. PM area optimization.

TABLE 5. Quantitative comparison after optimization.

Parameter	Initial Value	Optimized Value	Improvement
Flux Linkage$_{p-p}(Wb)$	0.08979	0.09967	11%
THD (%)	2.79	1.56	44.09%
F_d (N)	88.53	80.93	8.58%
$TF_{avg}(N)$	232.965	313.571	34.7%
TFD (kN/m^3)	318.491	429.11	34.7%
$TF_{rip}(N)$	76.13	62.89	21.05%

generating thrust force, while the other high-order harmonics produce only thrust ripple and gain losses.

$$Back - E.M.F = \frac{d\Phi}{dt} \tag{12}$$

The attraction between the stator's core and the mover's excitation causes detent force at no load (PM and FE). Detent force causes noise and vibration. If the attraction is stronger, noise and vibration will be increased, which in turn lower the TF_{avg}. The detent force of the proposed DSHEFSLM initial and optimized designs is shown in Fig. 17.

B. LOAD ANALYSIS

The thrust force of the proposed DSHEFSLM is maximized after the genetic optimization, as shown in Fig. 18. The TF_{avg} of 232.965N in the initial design was increased to 313.571N after optimization under the same electric and magnetic loading. Compared to the initial design, the optimized design has an increase of 34.6% in the TF_{avg} which is 31.2% more than the conventional design [26] average thrust force. The behavior of average thrust force versus armature and field current is observed in Fig. 19. The variation in TF_{avg} is observed while varying the armature current (I_{AC}) from 0 to 15A and the field current (I_{FE}) from 0 to 6A. The flux density plot: Fig. 20 shows the distribution of flux along all parts of the machine, indicating no saturation region.

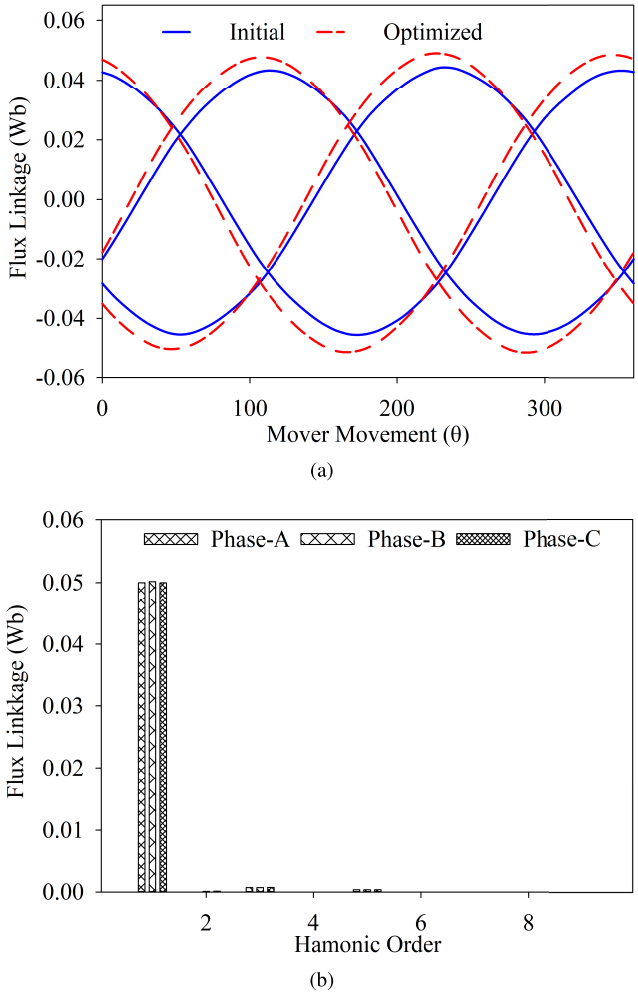

FIGURE 13. (a) Flux Linkage (b) Harmonics.

1) 3D SKEWING

Fig. 18 shows the ripples are a little higher in the thrust force. Since skewing is widely used to reduce the ripples in the thrust force, hence 3D skewing is employed in this study to minimize the ripples. Different skewed stators shown in Fig. 21 are employed to the mover, and the performance is observed. Skewing reduce ripples at the cost of a slight decrement in the average thrust force. 3D finite element analysis is done, and the impact of skewing step number on the performance is enlisted in Table 6. A stator three-step skewing structure is utilized for further analysis since the step skewing number should be minimal to simplify the implementation. With 3-step skewing, the ripples are reduced by 26% at the cost of 11% decrement in the average thrust force shown in Fig. 22.

2) DYNAMIC AND EFFICIENCY ANALYSIS

The force and power versus velocity curves for the proposed machine are calculated using the method [28], [29]. The force-velocity curve and the power-velocity curve are shown

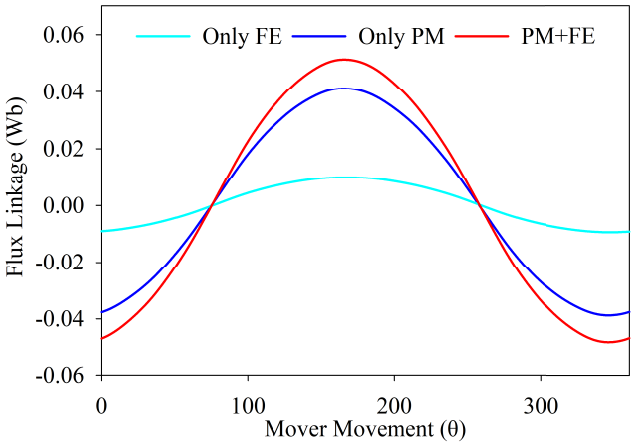

FIGURE 14. Influence of field current on no-load flux linkage.

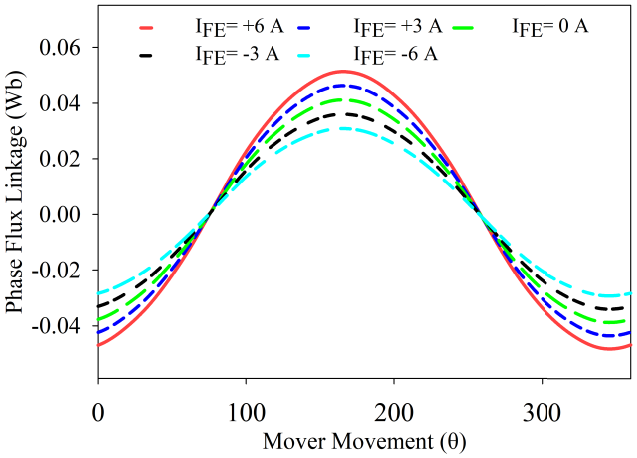

FIGURE 15. Flux regulation.

TABLE 6. Performance comparison of skewing steps.

Parameter	1-step	2-step	3-step	4-step	5-step
TF_{avg} (N)	313.57	301.19	282.50	278.37	272.91
Detent Force (N)	80.93	73.11	64.23	62.61	61.88
TF_{rip} (N)	62.89	57.31	49.91	47.08	45.89

in Fig. 23. From the analysis, it is clear that at the velocity of $3.59m/sec$, the proposed DSHEFSLM achieved a maximum TF_{avg} of $313.57N$ while the output power (P_{out}) reaches $1140W$. As force is inversely proportional to speed, the thrust will decrease at higher speeds, thereby maintaining a constant output power. Fig. 23 shows that the proposed DSHEFSLM has an excellent constant power operation capability.

The P_{out} of a linear machine is calculated by the product of the TF_{avg} and the associated velocity. At the same time, the input power is the sum of resultant P_{out} and the total losses, i.e., copper and iron losses. The losses are computed at various points on the force-velocity graph with different velocity and electric loading. The taken points are made up

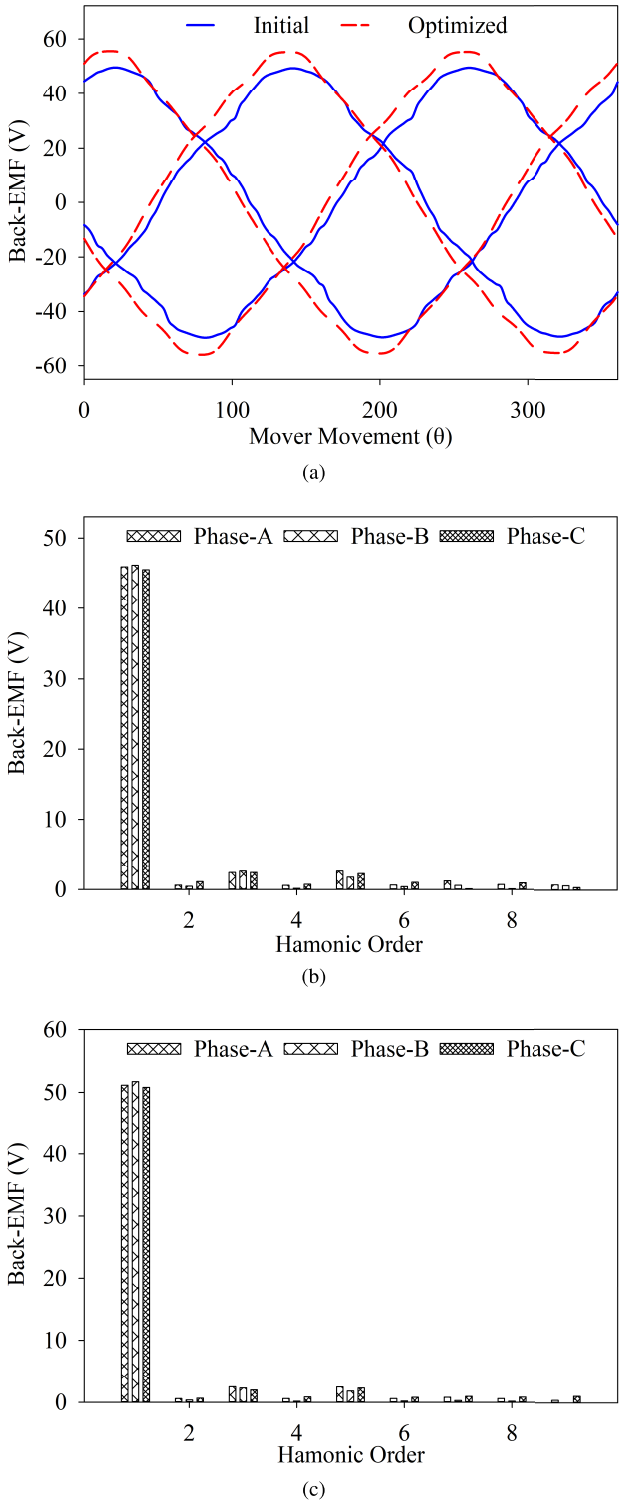

FIGURE 16. (a) Back-EMF (b) harmonics before optimization (c) harmonics after optimization.

of current and starting angles of current, as shown in Fig. 24. The copper losses are calculated using Eq. 15, whereas iron losses are determined using 2D FEA at all points specified. At point 1, the thrust force is maximum, and speed is lower; hence copper losses are higher, and iron losses are lower, i.e.,

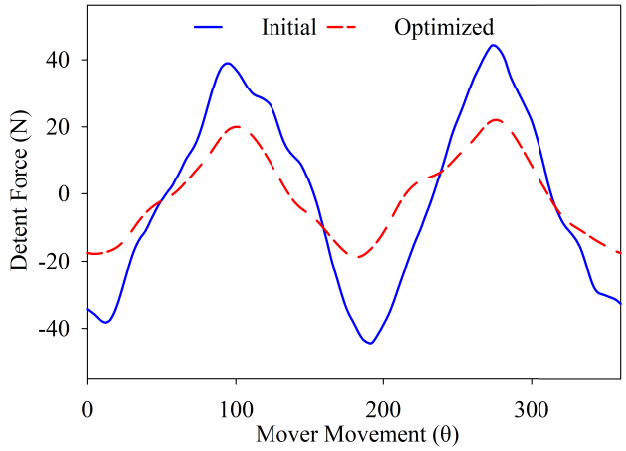

FIGURE 17. Detent force.

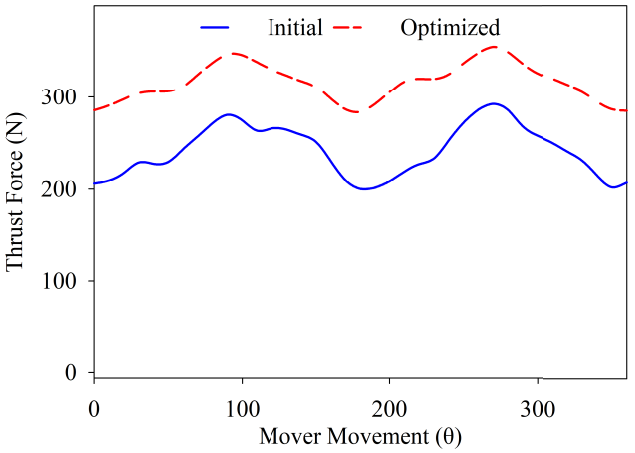

FIGURE 18. Thrust force.

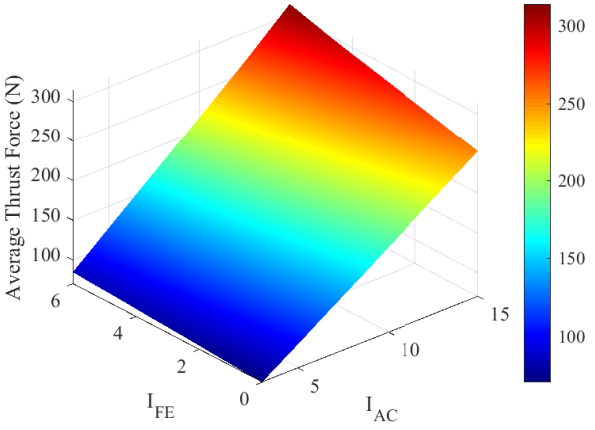

FIGURE 19. Average thrust force at different armature and field currents.

273W and 128W, respectively. At point 14, the iron losses are at a maximum (approximately 239W) because iron losses directly relate to speed while the copper losses were 123W, and hence efficiency is lower. The efficiency at all points of

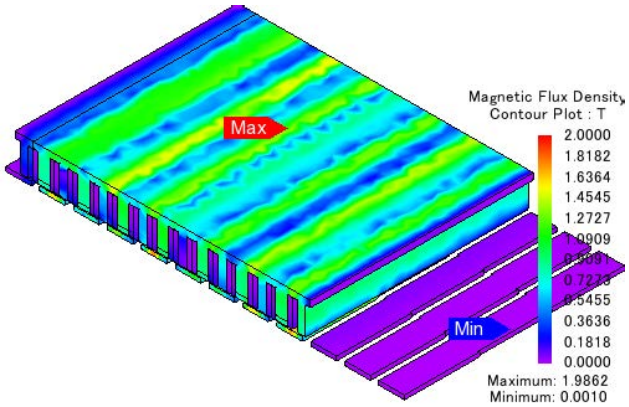

FIGURE 20. Flux density of the proposed design under loaded conditions.

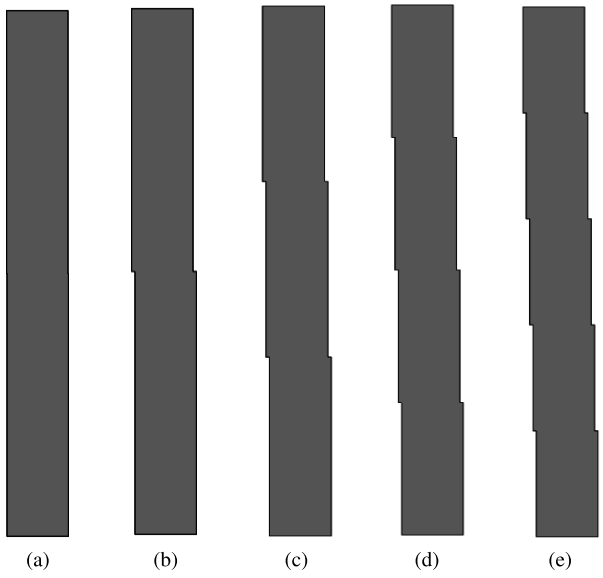

FIGURE 21. Skewing (a) 1-step (b) 2-step (c) 3-step (d) 4-step (e) 5-step.

the proposed machine is shown in Fig. 25.

$$P_{cu} = P_{cu}(AE) + P_{cu}(FE) \tag{13}$$

Also from [30],

$$P_{cu} = I\rho JL(NQ)(1000) \tag{14}$$

(13) becomes

$$P_{cu} = 2I\rho JL(NQ)(1000) \tag{15}$$

where I is current, ρ is resistivity ($\Omega - m$), J is current density (A/mm^2), L is length of wire (mm), N is number of turns, and Q is number of slot pairs.

C. LOSSES ANALYSIS

Different losses like iron, copper, and eddy current losses in PM are considered, and their effect on efficiency is observed. For the detailed loss analysis, one point at the maximum force region (P1), one point in the high-speed region (P14), and

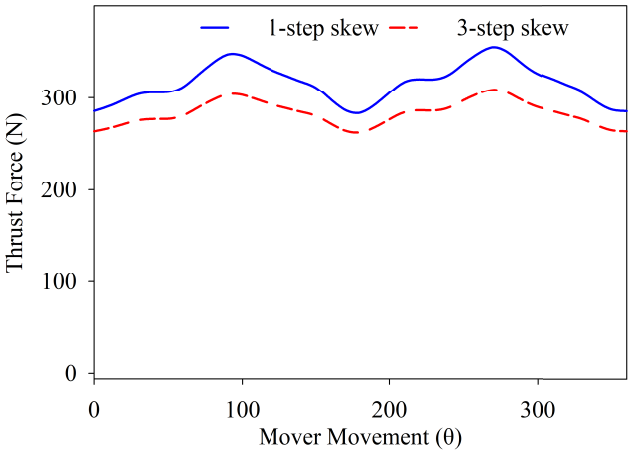

FIGURE 22. Thrust force after skewing.

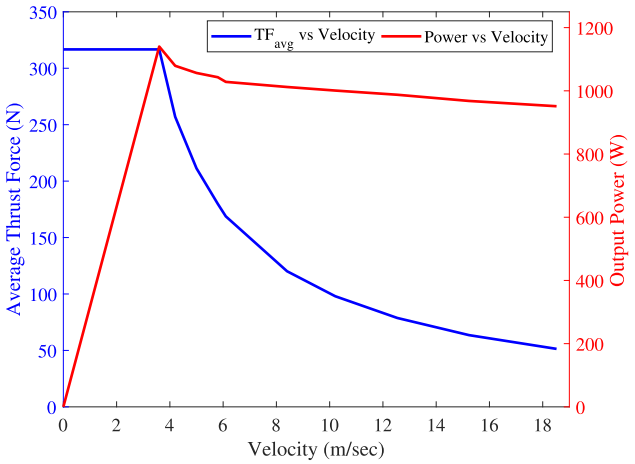

FIGURE 23. Average thrust force vs velocity and power vs velocity curves.

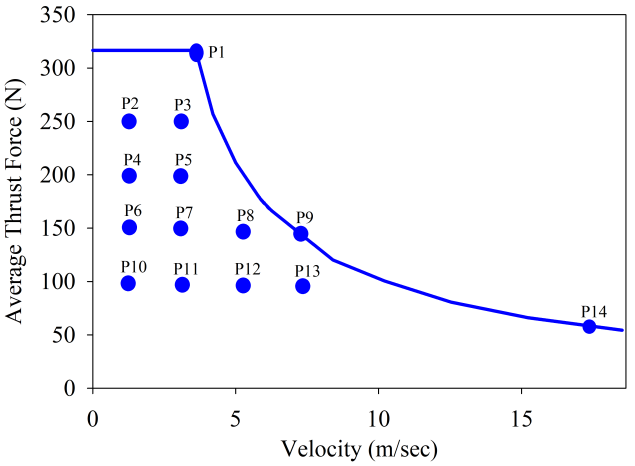

FIGURE 24. Efficiency at the calculated points.

three points in the best operation region (P4, P5, P6) are considered. Since iron losses are related to speed, at point 1, the speed is lower, and hence iron losses are smaller, and copper losses are higher. While at high speed (point 14), iron losses are higher, and copper losses are lower. Hence efficiency is

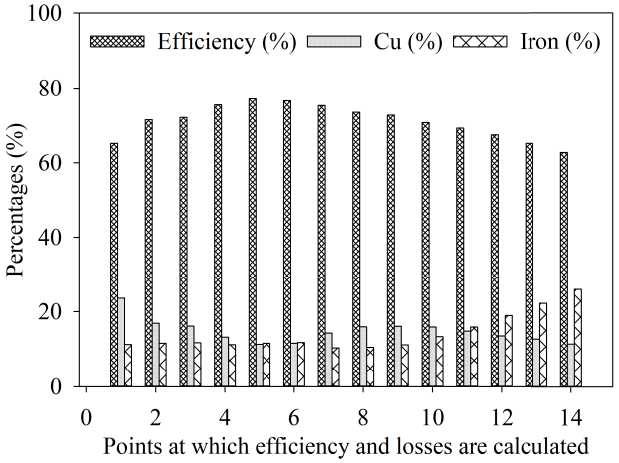

FIGURE 25. Efficiency of the proposed DSHEFSLM.

TABLE 7. Effect of PM losses on performance.

Parameter	P1	P4	P5	P6	P14
	Without PM eddy current losses				
Iron Losses (W)	128	107.32	88.45	91.42	239
FE Losses (W)	61.36	61.36	61.36	61.36	61.36
AC Losses (W)	211.64	89.11	87.89	88.54	61.68
Output Power (W)	1140.1	1056.5	1043.0	1035.7	1004.2
Efficiency (%)	64.83	75.60	77.21	76.70	63.98
	With PM eddy current losses				
PM Losses (W)	42.66	37.82	36.29	37.05	26.66
Output Power (W)	1079.91	1019.58	1010.91	999.13	996.87
Efficiency (%)	62.87	71.0	72.90	72.14	61.0

TABLE 8. Comparison with regular design.

Parameter	Proposed	Conventional
Rated Current (A)	15	15
Rated Velocity (m/s)	2	2
Air gap (mm)	0.8	0.8
Weight of PM (kg)	0.163	0.268
Weight of stator iron (kg)	0.945	0.945
TF_{avg} (N)	313.57 N	239 N
TF_{avg} per PM Volume	14.42 N/cm^3	6.68 N/cm^3
TFD	430.69 kN/m^3	328.27 kN/m^3

lower at these points. The FE losses are calculated using Eq. (14) and are constant because a constant excitation source is provided. When the eddy current losses of all PMs are considered, the TF_{avg} is decreased i.e. at point 1 the TF_{avg} was 313.57N initially when PM losses are considered the TF_{avg} dropped to 300.81N. The detailed losses analysis is given in Table 7. The power factor of the proposed machine is 0.76, lagging considering all the excitation sources.

VI. COMPARISON WITH REGULAR DESIGN

Finally, the proposed DSHEFSLM is compared with the conventional design, and the comparison results are shown

in Table 8. Both the designs use discrete stators, the same rated current, and the number of turns. In the proposed design, the volume of PM is reduced by 39.18% while achieving better performance as compared to the conventional design [26]. Further, the proposed design uses field excitation winding which adds flux controlling capability.

VII. CONCLUSION

A three-phase discrete stator HEFLM is investigated, which combines the high thrust density feature of permanent magnet machines and flux controlling features of FE machines. The proposed design has a single tooth armature and field excitation windings, thus minimizing copper losses. At both ends of the mover, auxiliary teeth are used to provide a path for the flux that is leaking from the ends of the mover. The results obtained through MEM show great agreement with FEA having an accuracy of 94.7%, thereby reducing computation time and drive storage. Genetic optimization is used to globally optimize the design parameters of the machine. Thrust force ripples were minimized by using 3D skewing. Dynamic analysis of the machine is done to determine the machine's performance over a wide range of speeds. A performance comparison between the proposed and the conventional design is carried out to display the superiority of the proposed design over the design proposed in the literature.

REFERENCES

[1] L. Xu, W. Zhao, J. Ji, G. Liu, Y. Du, Z. Fang, and L. Mo, "Design and analysis of a new linear hybrid excited flux reversal motor with inset permanent magnets," *IEEE Trans. Magn.*, vol. 50, no. 11, pp. 1–4, Nov. 2014.

[2] N. Ullah, F. Khan, W. Ullah, A. Basit, M. Umair, and Z. Khattak, "Analytical modelling of open-circuit flux linkage, cogging torque and electromagnetic torque for design of switched flux permanent magnet machine," *J. Magn.*, vol. 23, no. 2, pp. 253–266, Jun. 2018.

[3] C. F. Wang, J. X. Shen, Y. Wang, L. L. Wang, and M. J. Jin, "A new method for reduction of detent force in permanent magnet flux-switching linear motors," *IEEE Trans. Magn.*, vol. 45, no. 6, pp. 2843–2846, Jun. 2009.

[4] C.-C. Hwang, P.-L. Li, and C.-T. Liu, "Design and analysis of a novel hybrid excited linear flux switching permanent magnet motor," *IEEE Trans. Magn.*, vol. 48, no. 11, pp. 2969–2972, Nov. 2012.

[5] M. R. Dubois, H. Polinder, and J. A. Ferreira, "Magnet shaping for minimal magnet volume in machines," *IEEE Trans. Magn.*, vol. 38, no. 5, pp. 2985–2987, Sep. 2002.

[6] E. Sulaiman, T. Kosaka, and N. Matsui, "Design and performance of 6-slot 5-pole PMFSM with hybrid excitation for hybrid electric vehicle applications," in *Proc. Int. Power Electron. Conf.*, Jun. 2010, pp. 1962–1968.

[7] B. Gaussens, E. Hoang, M. Lécrivain, P. Manfe, and M. Gabsi, "A hybrid-excited flux-switching machine for high-speed DC-alternator applications," *IEEE Trans. Ind. Electron.*, vol. 61, no. 6, pp. 2976–2989, Jun. 2014.

[8] Z. Chen, B. Wang, Z. Chen, and Y. Yan, "Comparison of flux regulation ability of the hybrid excitation doubly salient machines," *IEEE Trans. Ind. Electron.*, vol. 61, no. 7, pp. 3155–3166, Jul. 2014.

[9] C. T. Liu, C. C. Hwang, P. L. Li, S. S. Hung, and P. Wendling, "Design optimization of a double-sided hybrid excited linear flux switching PM motor with low force ripple," *IEEE Trans. Magn.*, vol. 50, no. 11, pp. 1–4, Nov. 2014.

[10] T. Okada, H. Matsumori, T. Kosaka, and N. Matsui, "Hybrid excitation flux switching motor with permanent magnet placed at middle of field coil slots employing high filling factor windings," in *Proc. IEEE Energy Convers. Congr. Expo. (ECCE)*, Sep. 2018, pp. 4268–4274.

[11] W. Hua, G. Zhang, and M. Cheng, "Flux-regulation theories and principles of hybrid-excited flux-switching machines," *IEEE Trans. Ind. Electron.*, vol. 62, no. 9, pp. 5359–5369, Sep. 2015.

[12] Z. Zeng, Q. Lu, and Y. Ye, "Optimization design of E-core hybrid-excitation linear switched-flux permanent magnet machine," *Int. J. Appl. Electromagn. Mech.*, vol. 54, no. 3, pp. 351–366, Jul. 2017.

[13] H. Hua and Z. Q. Zhu, "Novel partitioned stator hybrid excited switched flux machines," *IEEE Trans. Energy Convers.*, vol. 32, no. 2, pp. 495–504, Jun. 2017.

[14] L. Zhang, Y. Fan, R. D. Lorenz, R. Cui, C. Li, and M. Cheng, "Design and analysis of a new five-phase brushless hybrid-excitation fault-tolerant motor for electric vehicles," *IEEE Trans. Ind. Appl.*, vol. 53, no. 4, pp. 3428–3437, Jul. 2017.

[15] Y. Gao, D. Li, R. Qu, X. Fan, J. Li, and H. Ding, "A novel hybrid excitation flux reversal machine for electric vehicle propulsion," *IEEE Trans. Veh. Technol.*, vol. 67, no. 1, pp. 171–182, Jan. 2018.

[16] M. Qasim, F. Khan, H. U. Jan, B. Ullah, B. Ejaz, and S. Hussain, "Novel partitioned primary linear hybrid excited flux switching machine with segmented secondary," in *Proc. Int. Conf. Emerg. Power Technol. (ICEPT)*, Apr. 2021, pp. 1–6.

[17] H. U. Jan, F. Khan, M. Qasim, B. Ullah, M. Yousaf, and Z. U. Islam, "Thermal and stress analysis of linear hybrid excited flux switching machine with modular stator," in *Proc. Int. Conf. Emerg. Power Technol. (ICEPT)*, Apr. 2021, pp. 1–6.

[18] B. Ullah, F. Khan, M. Qasim, H. U. Jan, B. Khan, and S. Khalid, "Design and analysis of consequent pole dual stator hybrid excited linear flux switching machine for rail transit system," in *Proc. Int. Conf. Emerg. Power Technol. (ICEPT)*, Apr. 2021, pp. 1–6.

[19] M. Qasim, F. Khan, B. Ullah, H. U. Jan, S. Hussain, and Z. U. Islam, "A novel double-sided linear flux switching machine with yokeless secondary for long stroke applications," in *Proc. Int. Conf. Emerg. Power Technol. (ICEPT)*, Apr. 2021, pp. 1–6.

[20] N. Ullah, F. Khan, A. Basit, W. Ullah, and I. Haseeb, "Analytical airgap field model and experimental validation of double sided hybrid excited linear flux switching machine," *IEEE Access*, vol. 9, pp. 117120–117131, 2021.

[21] B. Ullah, F. Khan, M. Qasim, B. Khan, A. H. Milyani, K. M. Cheema, and Z. Din, "Lumped parameter model and electromagnetic performance analysis of a single-sided variable flux permanent magnet linear machine," *Energies*, vol. 14, no. 17, p. 5494, Sep. 2021.

[22] B. Ullah, F. Khan, A. H. Milyani, N. Ahmad, and K. M. Cheema, "Design and analysis of dual-stator hybrid excited linear flux switching machine for long-stroke applications," *IET Electr. Power Appl.*, vol. 15, no. 12, pp. 1678–1691, Dec. 2021.

[23] Z. Zeng and Q. Lu, "Investigation of novel partitioned-primary hybrid-excited flux-switching linear machines," *IEEE Trans. Ind. Electron.*, vol. 65, no. 12, pp. 9804–9813, Dec. 2018.

[24] Z. Zeng, Y. Shen, Q. Lu, B. Wu, D. Gerada, and C. Gerada, "Investigation of a partitioned-primary hybrid-excited flux-switching linear machine with dual-PM," *IEEE Trans. Ind. Appl.*, vol. 55, no. 4, pp. 3649–3659, Jul. 2019.

[25] Y. Shen and Q. Lu, "Design and analysis of linear hybrid-excited slot permanent magnet machines," *IEEE Trans. Magn.*, vol. 54, no. 11, pp. 1–6, Nov. 2018.

[26] Q. Tan, M. Wang, and L. Li, "Analysis of a new flux switching permanent magnet linear motor," *IEEE Trans. Magn.*, vol. 57, no. 2, pp. 1–5, Feb. 2021.

[27] A. Chen, R. Nilssen, and A. Nysveen, "Analytical design of a high-torque flux-switching permanent magnet machine by a simplified lumped parameter magnetic circuit model," in *Proc. XIX Int. Conf. Electr. Mach. (ICEM)*, Sep. 2010, pp. 1–6.

[28] G. Qi, J. T. Chen, Z. Q. Zhu, D. Howe, L. B. Zhou, and C. L. Gu, "Influence of skew and cross-coupling on flux-weakening performance of permanent-magnet brushless AC machines," *IEEE Trans. Magn.*, vol. 45, no. 5, pp. 2110–2117, May 2009.

[29] Z. Q. Zhu, A. L. Shuraiji, and Q. F. Lu, "Comparative study of tubular partitioned stator permanent magnet machines," in *Proc. 10th Int. Conf. Ecol. Vehicles Renew. Energies (EVER)*, Mar. 2015, pp. 1–7.

[30] H. Hua, Z. Q. Zhu, and H. Zhan, "Novel consequent-pole hybrid excited machine with separated excitation stator," *IEEE Trans. Ind. Electron.*, vol. 63, no. 8, pp. 4718–4728, Apr. 2016.

BASHARAT ULLAH (Graduate Student Member, IEEE) received the B.S. degree in electronics engineering from the University of Engineering and Technology (UET), Peshawar, Pakistan, in 2015, and the M.S. degree in electrical engineering from the National University of Sciences and Technology (NUST), Islamabad, Pakistan, in 2017. He is currently pursuing the Ph.D. degree in electrical engineering with COMSATS University Islamabad, Abbottabad Campus. Since 2019, he has been a Research Associate with the Research in Design of Electric Machines (RiDEM) Laboratory. His research interests include design, optimization and analysis of rotary and linear hybrid excited flux-switching machines, linear actuators, and polyphase machines and their drives.

FAISAL KHAN (Member, IEEE) received the B.S. degree in electronics engineering and the M.S. degree in electrical engineering from COMSATS University Islamabad, Abbottabad Campus, Pakistan, in 2009 and 2012, respectively, and the Ph.D. degree in electrical engineering from Universiti Tun Hussein Onn Malaysia, Malaysia, in 2017. From 2010 to 2012, he was a Lecturer with the University of Engineering and Technology Peshawar, Abbottabad Campus, where he has been an Assistant Professor with the Department of Electrical Engineering, since 2017. He is the author of more than 130 publications, two patents and has received multiple research awards. His research interests include design of flux-switching, synchronous and DC machines. Furthermore, he is a member of IEEE Industrial Electronics Society and a member of IEEE-IES Electrical Machines Technical Committee.

AHMAD H. MILYANI received the B.Sc. (Hons.) and M.Sc. degrees in electrical and computer engineering from Purdue University, in 2011 and 2013, respectively, and the Ph.D. degree in electrical engineering from the University of Washington, in 2019. He is currently an Assistant Professor with the Department of Electrical and Computer Engineering, King Abdulaziz University, Jeddah, Saudi Arabia. His research interests include power systems operation and optimization, renewable and sustainable energy, power electronics, electric machines, electric vehicles, and machine learning.